cytes as a result of technical problems with the methods used. For instance, autofluorescence can interfere with the confocal microscopic analysis of immunofluorescence. In addition, earlier studies of post-MI regeneration were carried out using models that involved the permanent occlusion of coronary arteries, though clinical treatment for acute MI generally involves recanalization of infarct-related coronary arteries by thrombolysis or percutaneous angioplasty. Bearing these issues in mind, one of our aims in the present study was to use electron microscopy to determine whether intravenously injected autologous BM-MNCs can transdifferentiate into cardiomyocytes during post-MI repair in a rabbit ischemia–reperfusion model.

We also recently reported that the beneficial effects of granulocyte colony-stimulating factor are likely associated with the expression of repair-related cytokines as well as with cardiomyocyte regeneration [7], which suggests that BM-MNCs may also exert an effect on the expression of repair-related cytokines. Therefore, the second aim of this study was to determine whether expression levels of transforming growth factor (TGF)-β, a mediator stimulating collagen synthesis; matrix metalloproteinase (MMP)-1, a collagenase; or stromal cell-derived factor (SDF)-1, a chemoattractant known to recruit BM-MNCs into target tissues, correlate with post-MI repair after BM-MNC treatment.

2. Materials and methods

All the rabbits received humane care in accordance with the Guide for Care and Use of Laboratory Animals, published by the U.S. National Institutes of Health (NIH publication 8523, revised 1985). The study protocol was approved by the Ethics Committee of Gifu University School of Medicine, Gifu, Japan.

2.1. Autologous BM-MNCs

Male Japanese white rabbits weighing 1.9–2.5 kg were anesthetized by intravenous injection with 30 mg/kg of sodium pentobarbital. Approximately 10 ml of iliac BM was aspirated and suspended in 20 ml of RPMI-1640 medium (Sigma) containing 2000 U of heparin sodium. BM-MNCs were then isolated by centrifugation on a Ficoll gradient (JIMRO, Takasaki, Japan), and approximately 1.0×10^8 BM-MNCs were suspended in 2 ml of phosphate-buffered saline.

2.2. Ischemia–reperfusion infarct model and injection of BM-MNCs

One hour after the aspiration of BM, a 30-min ischemia and reperfusion protocol was carried out as previously described [7]. The rabbits were randomly assigned to either a BM-MNC or saline group, which were respectively administered the autologous BM-MNCs or 2 ml of saline via an ear vein after 5 h of reperfusion.

2.3. Protocol I: cardiac function and pathology

2.3.1. Echocardiography

The 90 rabbits in the BM-MNC and saline groups received trans-thoracic echocardiography (Aloka SSD4000) using a 7.5-mHz sector scan probe 7 days, 1 month and 3 months after the 30-min ischemia ($n=15$ in each group). LV anterior wall thickness (AWT, mm), posterior wall thickness (PWT, mm), body weight-corrected LV end-diastolic dimension (EDD/BW, mm/kg), and LV ejection fraction (EF, %) were measured. All measurements were made by two examiners (Y.M. and M.A.) blinded to the conditions.

2.3.2. General pathology

Following the echocardiography, each of the 90 rabbits was sacrificed with an overdose of pentobarbital after heparinization (500 U/kg), after which body weight and LV weight were measured. The LV was then fixed in 10% buffered formalin and sliced into 7 transverse sections parallel to the atrio-ventricular ring from the apex to the base. The slices were embedded in paraffin, cut to a thickness of 4 μm, and stained with hematoxylin and eosin (HE) and Sirius red. For transversely sliced preparations with infarction, the LV wall areas, infarcted areas, non-infarcted areas, and Sirius red-positive collagen areas were calculated using an image analyzer connected to a light microscope (LUZEX-F, NIRECO, Tokyo) and expressed as mm^2/slice/body weight (kg). Comparisons were made by two persons (Y.M. and M.A.) blinded to the conditions.

2.3.3. Immunohistochemistry

Using the indirect immunoperoxidase method, immunohistochemical staining was carried out with the following monoclonal antibodies (mAbs) that all cross-react with rabbit tissues: mouse anti-rabbit sarcomeric actin mAb (1:75; DAKO), mouse anti-human endothelial cell CD31 mAb (1:100; DAKO), mouse anti-human α-smooth muscle actin mAb (1:250; DAKO, 1A4), mouse anti-macrophage mAb (1:100; DAKO, RAM11), mouse anti-human MMP-1 mAb (1:500; Daiichi Fine Chemical, F-67), mouse anti-human TGF-β mAb (1:2000; Oxford Biotechnology.) and mouse anti-human/mouse SDF-1 mAb (1:120; R&D Systems). Morphometric analyses were carried out by two persons (Y.M. and G.T.) blinded to the conditions.

2.4. Protocol II: DiI-labeling of BM-MNCs, electron microscopy, laser scanning confocal microscopy and Western blotting

BM-MNCs were isolated from 12 rabbits as described above and then incubated for 30 min at 37 °C. To label the

cells with 1,1′-dioctadecyl-1 to 3,3,3′,3′-tetramethylindocarbocyanine perchlorate dye (DiI, Molecular Probes), 25 μl of a 2-mg/ml solution of DiI in dimethyl sulfoxide (Wako, Japan) was added to the BM-MNCs from 6 of the rabbits [8,9]. Thereafter, those 12 rabbits plus 6 in a saline group were subjected to the 30-min ischemia and reperfusion protocol, and after 5 h of reperfusion, the autologous BM-MNCs, with or without DiI, or 2 ml of saline (6 rabbits in each group) were injected via an ear vein. Seven days post-MI, the rabbits were sacrificed under anesthesia, and the hearts were immediately excised and placed in iced PBS (less than 4 °C) and cut transversely at the center of the infarcted anterior LV wall. The upper half was subsequently used for electron microscopy and laser-scanning confocal microscopy, and the lower half was used for Western blot analysis.

Immediately after sacrifice (within 1 min), myocardial tissue from the upper infarcted anterior LV wall (AW-MI) and non-infarcted posterior LV wall (PW-NMI) of each heart was cut into 1-mm cubes, fixed in 2.5% glutaraldehyde in 0.1 mol/L phosphate buffer (pH 7.4) at 4 °C for 4 h, and post-fixed in 1% buffered osmium tetroxide for 2 h. The samples were then dehydrated through a graded ethanol series and embedded in epoxy resin. One serial thin section (80 nm) was conventionally double-stained with uranylacetate for 10 min and lead citrate for 4 min and used for an electron microscopic (H-800, Hitachi) detection of ultrastructure. Another thin section stained with lead citrate for 1 min was used for the detection of DiI particles at magnifications greater than 20,000×.

In addition, other tissue samples obtained from the upper AW-MI and PW-NMI (three samples each, approximately 3 × 3 × 2 mm) were embedded in OCT compound (Miles Scientific), snap-frozen in liquid nitrogen and cut into 6-μm-thick sections using a cryostat for immunohistochemical analysis. Immunofluorescence microscopy was carried out using mouse anti-troponin I mAb (1:5000; CHEMICON), mouse anti-human endothelial cell CD31 mAb, and mouse anti-human α-smooth muscle actin mAb. Nuclei were stained with Hoechst 33342. The tissues were observed using a laser-scanning confocal microscope (LSM510 NLO, ZEISS, Tokyo), which enabled simultaneous analysis of the relationship between three different fluorescence and phase contrast images. Morphometric analyses were performed by two persons (Y.M. and M.A.) blinded to the conditions.

For Western blot analysis, tissues (approximately 200 mg) obtained from the center of the lower AW-MI and PW-NMI were snap-frozen in liquid nitrogen immediately after sacrifice. For the measurement of MMP-1, TGF-β and SDF-1, 50 mg of frozen tissue obtained from the hearts of sham, saline and BM-MNC-treated rabbits were homogenized in lysis buffer and centrifuged for 10 min at 10,000×*g* and 4 °C. MMP-1, TGF-β and SDF-1 were measured by Western blot analysis using the same Abs described for Protocol I. Signals were quantified by densitometry.

2.5. Protocol III: in vitro study

BM-MNCs and cultured adult cardiomyocytes [10] were left untreated or pretreated with DiI for 30 min at 37 °C, after which they were incubated for 7 days at 37 °C and processed for electron microscopy (fixed in 2.5% glutaraldehyde in 0.1 mol/L phosphate buffer [pH 7.4] for 30 min, post-fixed in 1% buffered osmium tetroxide for 1 h, dehydrated through graded ethanol and embedded in epoxy resin).

2.6. Statistical analysis

All values are presented as means ± S.D. Differences between the saline and BM-MNC groups were assessed by two-way repeated-measures analysis of variance (ANOVA), followed with a post hoc Tukey–Kramer's test. Linear regression techniques were used to evaluate the correlation between pathological/echocardiographic parameters and the expression of cytokines. Values of $p < 0.05$ were considered significant.

3. Results

3.1. Mortality

All rabbits in the saline and BM-MNC groups survived until sacrificed 7 days, 1 month or 3 months post-MI.

3.2. Echocardiography

LV anterior wall thickness 1 and 3 months after MI was significantly greater in the BM-MNC group (2.2 ± 0.2 and 2.3 ± 0.2 mm, respectively) than the saline group (1.6 ± 0.2 and 1.8 ± 0.2 mm, respectively), but there was no significant difference in posterior wall thickness between the two groups at any time point as shown in Fig. 1a and b. In the saline group, additionally, EFs were significantly lower and EDD/BWs were significantly higher 1 month and 3 months post-MI than before infarction (Fig. 1c and d). These adverse effects were significantly attenuated in the BM-MNC group, indicating an improved LV function and reduced remodeling (Fig. 1c and d).

3.3. General histology

Seven days post-MI, the infarcted areas showed mostly granulation with numerous myofibroblasts and small vessels in both the saline and BM-MNC groups. In addition, residual necrotic areas were observed in the centers of the granulated tissues. The numbers of small arteries positive for α-smooth muscle actin (a specific marker of smooth muscle cells) and microvessels positive for CD31 (a specific endothelial marker) were significantly larger in the BM-MNC group than the saline group (Fig. 2a and b), as were numbers of macrophages positive for RAM 11 (a specific

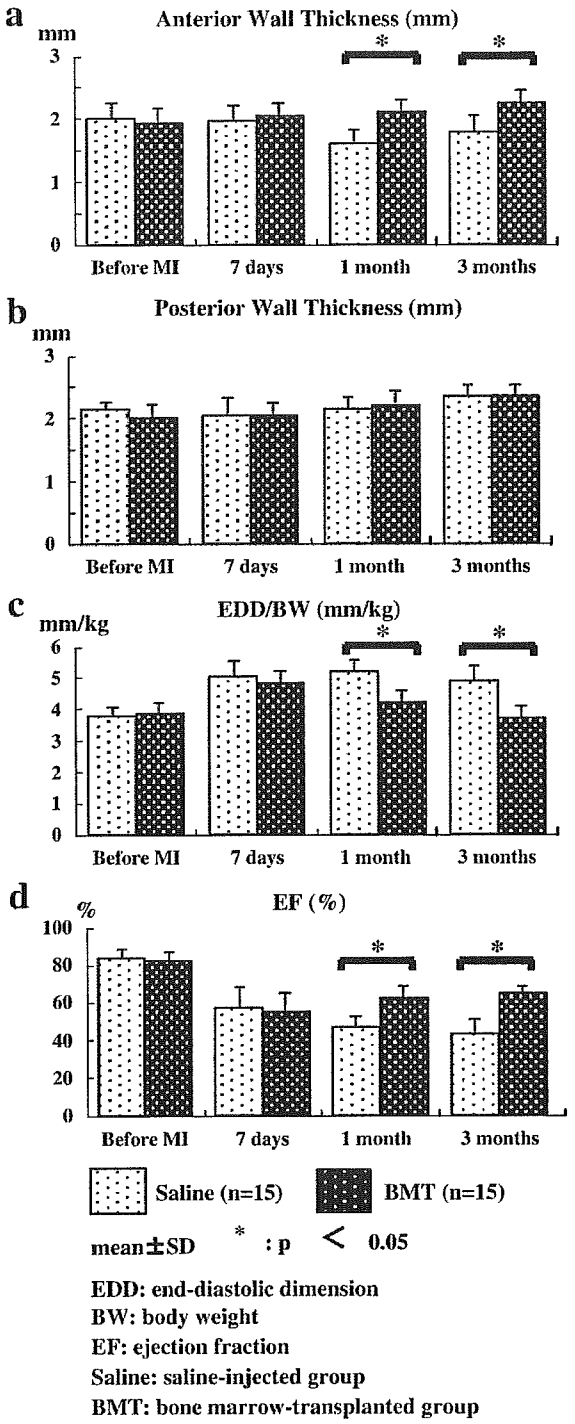

Fig. 1. BM-MNC treatment improves echocardiographic findings. AWTs, PWTs, EFs and EDD/BW ratios obtained 7 days, 1 month and 3 months post-MI.

marker of macrophages) and multinuclear giant cells (Fig. 2c). On the other hand, the respective transverse diameters of the cardiomyocytes in the AW-MI and PW-NMI were similar in the saline and BM-MNC groups, though the size of the cells was significantly greater in the AW-MI than the PW-NMI in each group (Fig. 3a).

One and three months post-MI, LV weight and LV wall area were also similar between the BM-MNC and saline groups (Fig. 3b and c), and the infarcted areas showed scar tissue comprised of collagen and fatty tissue in both the saline and BM-MNC groups. When the LV walls were stained with HE and the collagen with Sirius red, however, the old infarcts were found to be significantly smaller in the BM-MNC group than in the saline group (Fig. 3d and e). Conversely, the non-infarcted areas were significantly larger in the BM-MNC group (Fig. 3f). In both groups, the numbers of CD31-positive capillaries, α-smooth muscle actin-positive small arteries, and RAM 11-positive macrophages were markedly smaller than the numbers seen 7 days after infarction and were similar (Fig. 2a–c).

3.4. Electron microscopy

An extensive search using electron microscopy revealed unfamiliar mononuclear cells in the AW-MI of BM-MNC hearts 7 days post-MI. Differing from normal adult cardiomyocytes with mature sarcomeres (Fig. 4a), these cells were relatively large and electron-lucent, and their cytoplasm lacked cross-striations, but was loosely or tightly packed with myofilaments, the size of which suggested they were thin filaments (Fig. 4b1). Although reminiscent of myofibroblasts or smooth muscle cells, these cells had several features that were specific to immature cardiomyocytes: first, they were connected to one another by intercalated discs, a specific structure of striated muscle cells, including cardiomyocytes, and the intercalated discs contained distinct desmosomes and gap junctions (Fig. 4b2, c2, e and f). In intercalated discs, we did not detect clear fascia adherence; the absence is probably due to not-well-developed myofilaments in the cytoplasm; and second, Z disc-like structures were scattered among the myofilaments (Fig. 4c, c1 and d). There were small structures that appeared like myofilaments tied up into bundles in the vicinity of intermingling thick filaments, a configuration similar to the developing Z discs observed in fetal hearts [11]. Other, apparently more differentiated, cell types were also found, which contained better developed, but still not complete, Z discs (Fig. 4f). Such cells formed occasional clusters (Fig. 4b and c). Taken together, these findings suggest the presence of myocyte-like cells undergoing differentiation in the AW-MI of BM-MNC hearts, though their numbers were small: on average, the number of observed myocyte-like cells was 4.6±3.9/heart in the BM-MNC group and 0±0/heart in the saline group.

To determine whether these myocyte-like cells were derived from bone marrow cells, we first examined cultured BM-MNCs and isolated adult cardiomyocytes that had been incubated with DiI. We detected no DiI in specimens conventionally double-stained with uranyl acetate and lead citrate for electron microscopic examination (Fig. 5a).

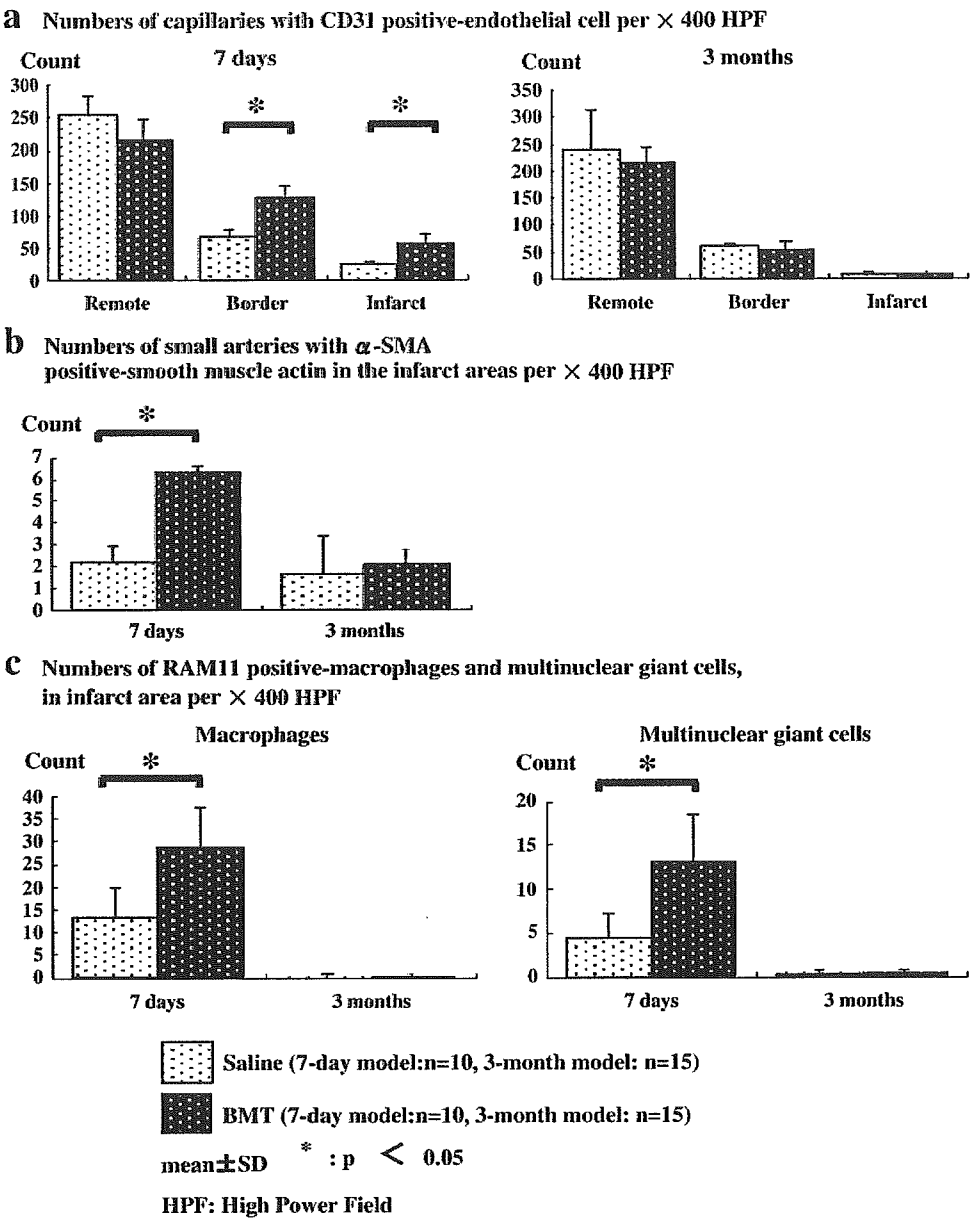

Fig. 2. Interstitial cell densities. The numbers of CD31-positive capillaries, α-smooth muscle actin-positive small arteries, RAM 11-positive macrophages and giant cells observed 7 days post-MI. Cells were counted in each of 15 serial fields per rabbit under a light microscopy. The border zone was defined as surviving myocardial tissue areas within 1 mm of infarcted areas.

However, when specimens were stained for only a short time with lead citrate alone, DiI was detected as 5-nm particles that accumulated within the cells and were scattered in the cytoplasm, mitochondria and lysosomes (Fig. 5b–d). These particles were not observed in cells that were not incubated with DiI. When DiI-labeled BM-MNC and control hearts were examined using the same method, DiI particles were detected in a total of 20 myocyte-like cells in the BM-MNC hearts (Fig. 5e–f) and were also occasionally found in pericytes present in the infarcted area (Fig. 5g and h). In addition, there was no evidence of DiI particles in BM-MNC and saline hearts not labeled with DiI.

3.5. Confocal microscopy

Within tissue sections obtained from the AW-MI of DiI-labeled BM-MNC hearts 7 days after MI, 0.14±0.13% of troponin I-positive (green) cells were also DiI-positive (red), and these cells formed a cluster (Fig. 6b). In addition, 0.05±0.04% of the cells positive for α-smooth muscle actin

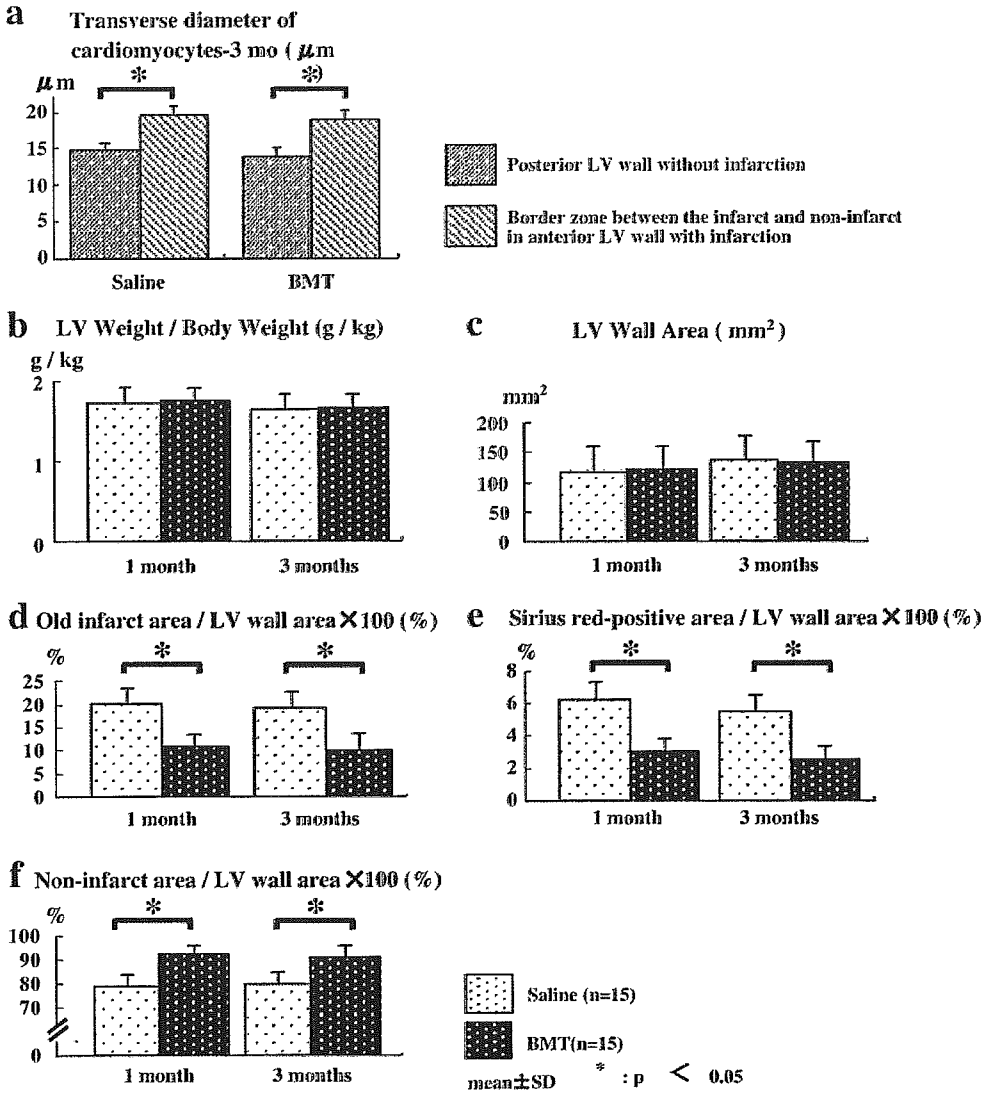

Fig. 3. BM-MNC treatment reduces infarct size and increases non-infarcted area. Shown are LV weight, LV wall area, cardiomyocyte size, non-infarcted area and old infarct areas. The border zone was defined as in the legend to Fig. 2.

and 0.3±0.3% of cells positive for CD31 were also positive for DiI.

3.6. TGF-β, MMP-1 and SDF-1

Immunohistochemical analysis showed TGF-β to be expressed in endothelial cells, smooth muscle cells and myofibroblasts (Fig. 7 and Supplementary data 1). In the saline groups, the level of expression within the infarcted areas was highest 7 days and 1 month post-MI (2.2±0.3 and 2.4±0.3, respectively) but had declined by 3 months (1.6±0.8) (Fig. 8a). There was significantly less expression of TGF-β in the infarcted areas of BM-MNC hearts 7 days and 1 month post-infarction (1.1±0.4 and 1.2±0.8, respectively), but by 3 months, the level of expression in the BM-MNC group (1.4±0.7) was similar to that in the saline group (1.6±0.8).

MMP-1 was expressed in cardiomyocytes located at the border between the infarcted area and salvaged myocardial tissues (Fig. 7). In the saline group, the level of MMP-1 expression was highest 7 days and 1 month post-MI (2.6±0.4 and 2.4±0.6, respectively), but dropped significantly by 3 months (1.4±0.8) (Fig. 8b). As was seen with TGF-β, there was significantly less expression of MMP-1 in the BM-MNC group 7 days and 1 month post-MI (1.1±0.5 and 1.3±0.8, respectively).

Expression of SDF-1 was observed in endothelial cells, vascular smooth muscle cells, myofibroblasts and interstitial fibrous tissues within the infarcts 7 days post-MI. (Fig. 7 and Supplementary data 1) The level of SDF-1

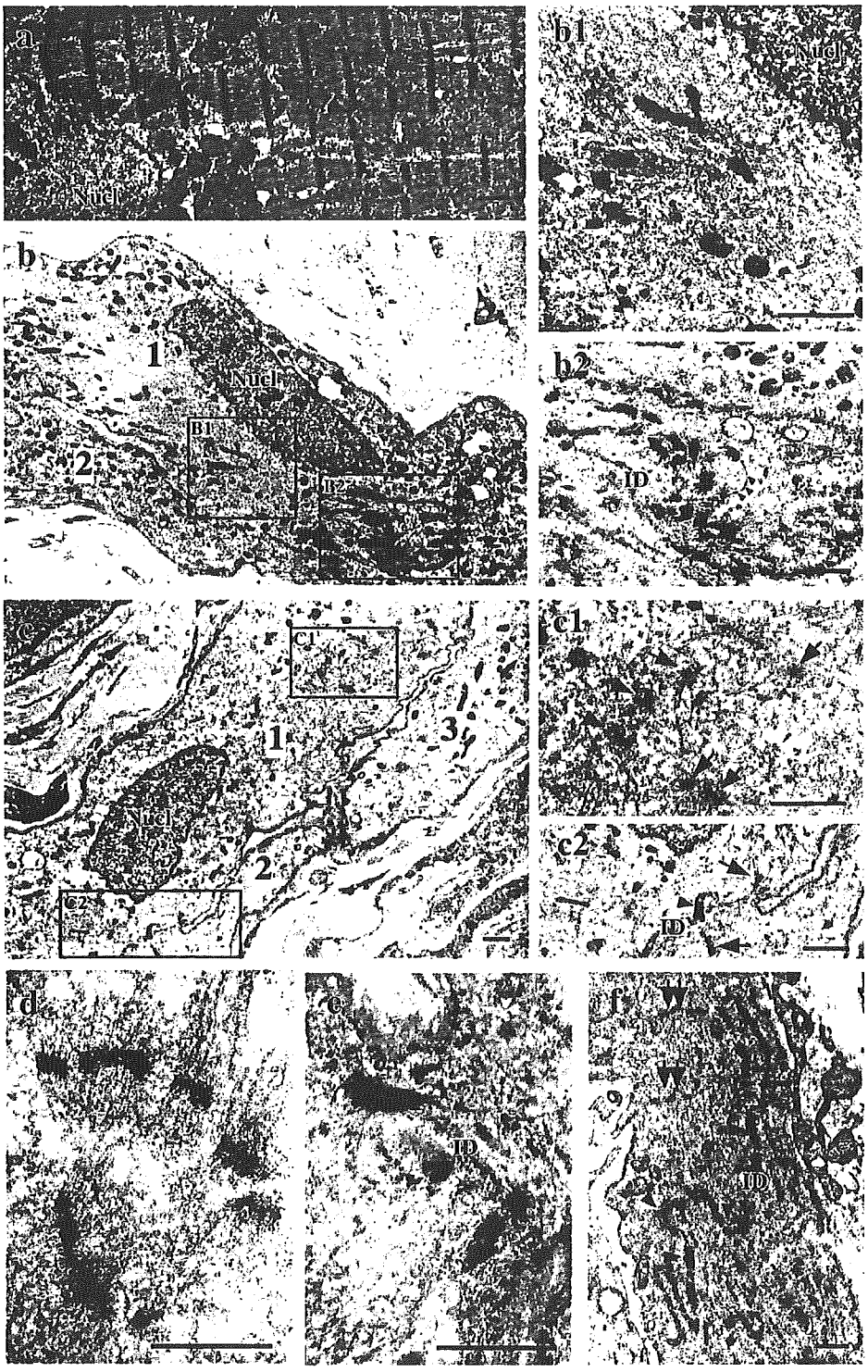

Fig. 4. Ultrastructure of myocyte-like cells in the infarcted anterior LV wall of the BM-MNC group 7 days post-MI. (a) Normal adult cardiomyocyte showing characteristic striations and mature sarcomeres. (b) Relatively large and electron-lucent immature cells; (b1 and b2) highly magnified images of the boxed portions in panel (b). Note the thin filaments filling the cytoplasm (b1), and that the cells were perpendicularly connected to one another by well-developed intercalated discs (ID) (b2). Small triple arrowheads indicate gap junctions (b2). (c) Z disk-like structures in myocyte-like cells. (c1 and c2) Highly magnified photographs of the boxed portions of panel (c); the cells contain Z disc-like structures (arrows) scattered in the cytoplasm (c1). An arrowhead indicates desmosome-containing intercalated discs (c2). (d and e) Myocyte-like cells; High magnification of Z disc-like structures (d) and desmosomes within an intercalated disc (e). (f) More developed Z discs (double arrows) connected to one another by intercalated discs (ID). Black and white arrowheads indicate, respectively, desmosomes and gap junction in ID.

expression was significantly higher in the BM-MNC group (2.6±0.3) than in the saline group (0.8±0.3) (Fig. 8c). No expression was detected in either group 1 and 3 months post-MI.

As shown in Fig. 9, Western blot analysis 7 days post-MI showed that the enhanced expression of TGF-β in the LV anterior wall with infarction and the LV posterior wall in the saline group was significantly down-regulated in the BM-MNC group. Pro-MMP-1 expression was enhanced in the LV anterior wall of the saline group and the enhancement was significantly inhibited in the BM-MNC group. The enhanced expression of SDF-1 in the LV anterior wall 24 h after MI disappeared 7 days later in the saline group. In the BM-MNC group, however, SDF-1 was markedly expressed in both the LV anterior and posterior walls 7 days post-MI.

3.7. Correlation between cytokine expression, LV function and remodeling, and old infarct size

One month after infarction, levels of TGF-β and MMP-1 were negatively and significantly correlated with AWT/PWT ratios and EFs. They were also positively and significantly correlated with EDD and old infarct size (Fig. 8a and b).

4. Discussion

4.1. Injected BM-MNC-derived myocyte-like cells and pericytes—limitation of electron microscopic analysis

Our electron microscopic analysis suggests that very immature (fetal) as well as relatively mature mononuclear cardiomyocytes formed clusters in the infarcted area of the anterior LV myocardium in the hearts of rabbits receiving BM-MNCs following acute MI. These cells differed from cardiomyocytes fused with stem cells which retain the fine ultrastructure and cross-striations of mature cardiomyocytes and are multinuclear [6,12–14]. Each of the myocyte-like cells was positive for DiI particles (a marker of injected BM-MNCs), and DiI particles were observed in pericytes, as well. This finding is consistent with the idea that intravenously injected BM-MNCs are able to transdifferentiate into both myocyte-like cells and pericytes. As BM-MNCs include both hematopoietic and mesenchymal stem cells, it is unclear from which of these cell types the BM-MNC-derived myocyte-like cells are derived.

However, a limitation of electron microscopic analysis is that only very small areas of the tissue samples are actually observed. For that reason, we were unable to precisely determine the total numbers of BM-MNC-derived cells present in infarcted hearts. For the same reason, we cannot rule out the possible existence of cardiomyocytes fused with BM-MNCs. Conversely, negative electron microscopic findings do not imply that the cells are absent.

In the present study, our confocal light microscopic analysis of DiI fluorescence as well as electron microscopic analysis indicated that the incidence of BM-MNC-derived cardiomyocytes was very low in post-MI hearts. However, recent observations reported from several laboratories indicate that following i.v. injection [15], only a very small percentage of cells are actually retained in the heart. Thus, the very small percentage of the regenerated cells is not surprising. However, this observation does not prove that a higher degree of myocyte regeneration cannot be achieved following intramyocardial or intracoronary injection of bone marrow cells. Nor can this observation be extrapolated to imply that bone marrow cell therapy leads to minimal regeneration of cardiomyocytes.

4.2. Up-regulation of SDF-1

Up-regulation of SDF-1 expression was seen in myocardial tissues in the BM-MNC group 7 days post-MI. Given that SDF-1 is able to recruit circulating bone marrow-derived cells into targeted tissues [16–18], this up-regulation may be related to the appearance of BM-MNC-derived cardiac cells.

4.3. Mechanisms of improved LV function and reduced infarct size

A reduction in infarcted area via the formation of less scar tissue could only be supported by an increase in size of the preexisting myocytes and/or the formation of new myocyte, since the total LV area and weight were similar. In the present study, this reduction was equivalent to approximately 10% of the LV area. First, it is clear that the number of regenerated cardiomyocytes within infarcted areas was too small to explain the 10% increase in non-scarred areas. Second, the increase in LV area approximately 10% corresponds to the increase of approximately 3% in the transverse size of cardiomyocytes. Although a significant difference in the transverse size of cardiomyocytes was not observed between the BM-MNC and saline groups in the present study, there is no reliable method of detecting precisely the minimum increase in the transverse size of cardiomyocytes at present. Therefore, the increase in non-scarred areas would be considered to be due to a minimum hypertrophy of preexisting myocytes rather than the regeneration of cardiomyocytes. Further investigation is warranted.

Because the mediators contributing to cardiac development and remodeling are expressed only transiently and may thus be absent from healed and/or newly formed cardiac tissue [19], we assessed their levels at several points post-MI, with the aim of evaluating the causal relationship between changes in cytokine levels and LV function. Expression of TGF-β and MMP-1 is reportedly up-regulated following MI [20–22]. Similarly, in the

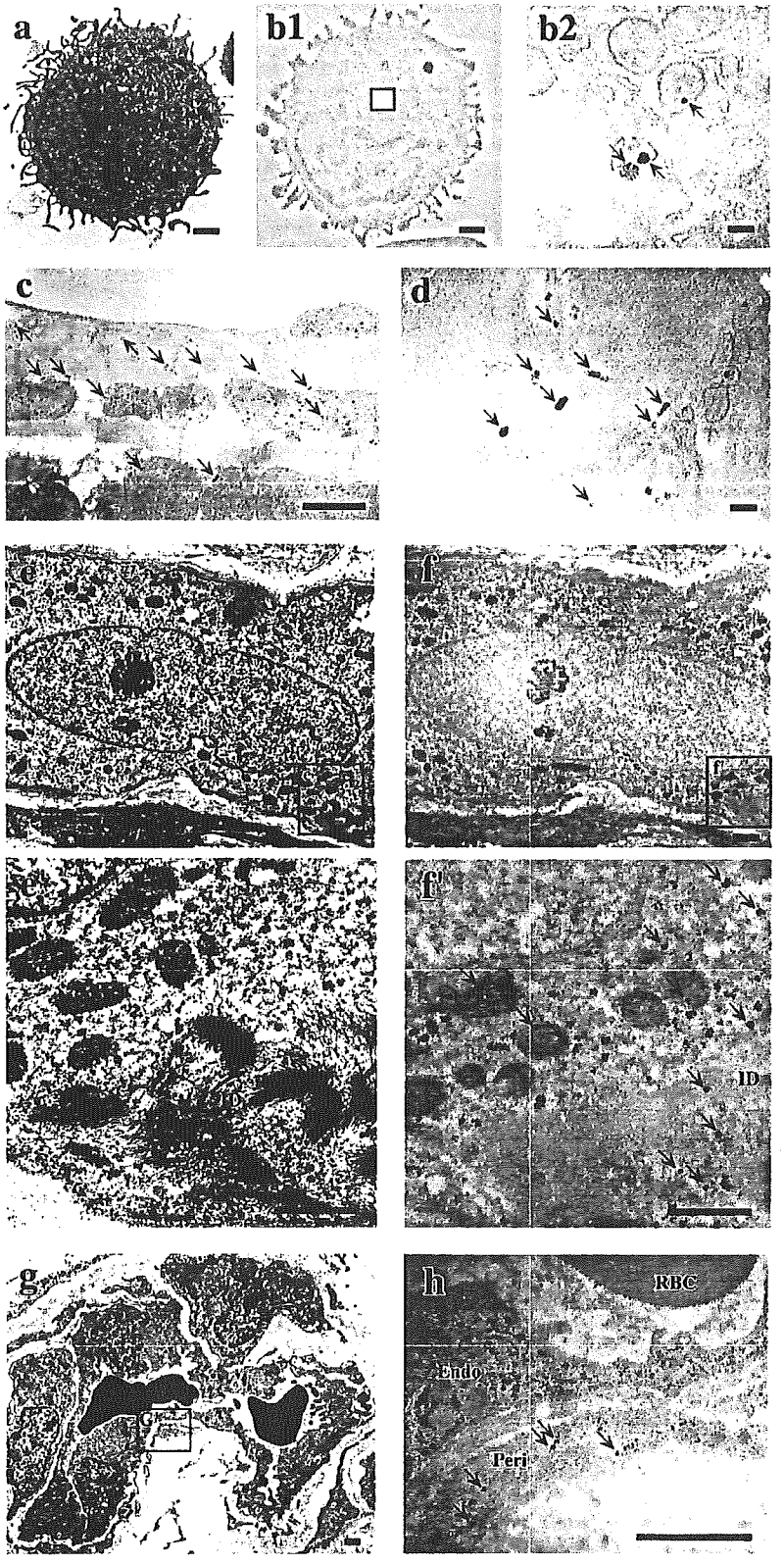
a
b1
b2
c
d
e
f
f'
e'
ID
g
h
RBC
Endo
Peri

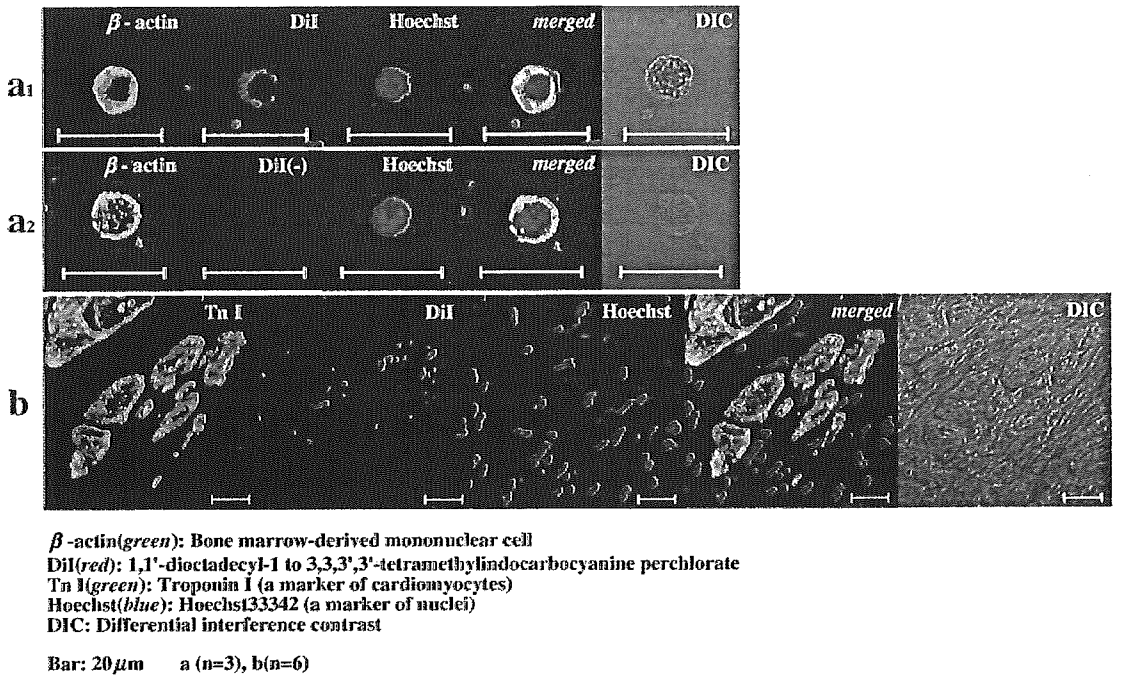

Fig. 6. Laser-scanning confocal microscopic findings. Red immunofluorescence is seen in a DiI-labeled BM-MNC (a1) but not in a BM-MNC without DiI labeling (a2). Note the characteristic punctate distribution of DiI in the cytoplasm. (b) Cluster formed by TnI- and DiI-positive BM-MNC-derived cardiomyocytes.

saline group, their expression was up-regulated 7 days and 1 month post-MI. However, we found that this up-regulation was significantly attenuated by administration of BM-MNCs. That the improvement in LV function was not seen in the BM-MNC group until 1 month post-MI means that the down-regulation of cytokines in the BM-MNC group 7 days post-MI preceded the improved LV function. Moreover, the reduction in TGF-β and MMP-1 levels seen 1 month after infarction correlated significantly with the improvement in indicators of LV function (EDD, EF and AWT/PWT ratios), which is consistent with the earlier finding that inhibition of TGF-β or MMP improves cardiac function in failing hearts [21,23,24]. We therefore suggest that the down-regulation of TGF-β and MMP-1 likely contributed to the improved LV function seen in the BM-MNC-treated animals.

Finally, the old infarcts were smaller in the hearts from rabbits administered BM-MNCs than in those from rabbits administered saline, which is indicative of a reduction in the amount of collagen present at the infarct site. This reduction in infarct size is also consistent with the lower levels of TGF-β expressed in BM-MNC hearts, given the ability of TGF-β to induce collagen synthesis. Also, inhibition of apoptosis by a paracrine effect of BMT would be a possible mechanism for the beneficial effect, because the presence has been reported [25].

4.4. Transient increases in vessel density

Generally, vascular regeneration during the chronic stage of MI is enhanced by the injection of BM-MNCs [26]. In the present study, however, the increase in vascular density seen at the subacute stage (7 days post-MI) in the BM-MNC group disappeared during the chronic stage (3 months post-MI). This likely reflects the fact that we used a model of ischemia–reperfusion, which produced moderate infarctions, and differed from the models used in most earlier studies, which involved permanent occlusion

Fig. 5. Electron micrographs showing DiI particles within the ultrastructure. (a) DiI-labeled mononuclear bone marrow cell treated with a conventional electron stain. DiI particles are undetectable, hidden by other cytoplasmic structures. (b1 and b2) Highly magnified micrographs of DiI-labeled, unstained mononuclear bone marrow cells; accumulated DiI particles (arrows) can be clearly seen. (c) DiI-labeled, unstained adult cardiomyocyte in culture; arrows indicate DiI particles. (d) Highly magnified cytoplasm of a DiI-labeled adult cardiomyocyte in culture; DiI particles are indicated by arrows. (e) Conventionally stained myocyte-like cells in the infarcted area 7 days post-MI. (e') Highly magnified micrograph of the boxed portions of panel (e) showing the intercalated disc (ID). (f) Serial section of the myocyte-like cells shown in panel (e) stained for a short period with only lead citrate. (f') Highly magnified photograph of the boxed portions of panel (e) showing abundant DiI particles (arrows). (g) A conventionally stained capillary vessel in the infarcted area 7 days post-MI. (h) Highly magnified photograph of a capillary vessel in a serial, unstained section of the vessel in panel (g). This portion roughly corresponds to the boxed area of panel (g). DiI particles are seen in the pericyte (arrows). ID, intercalated disc; RBC, red blood cell; Endo, endothelial cell; Peri; pericyte. Bars, 0.1 μm in panels (b1), (b2) and (d); 1 μm in the other panels.

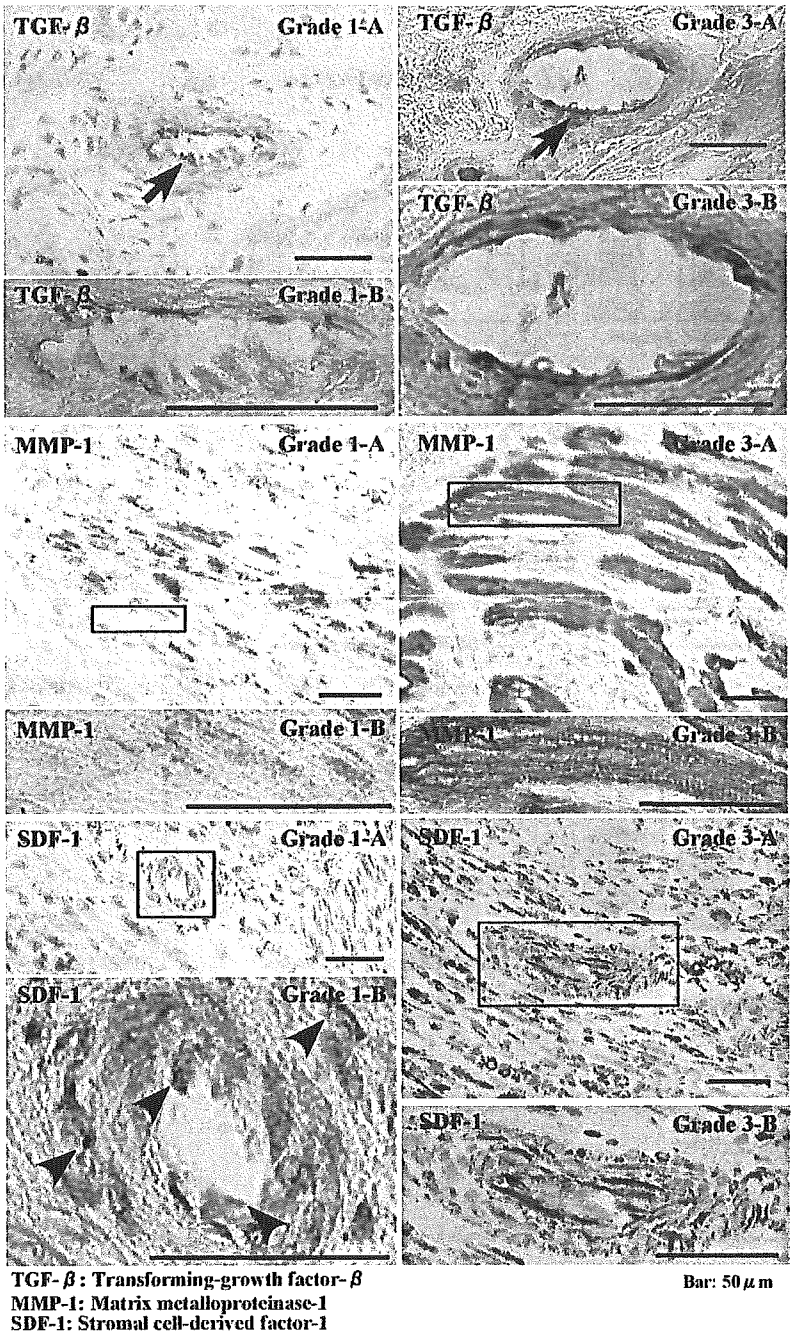

Fig. 7. Immunohistochemical analysis of repair-related cytokines. Immunolabeling of TGF-β and SDF-1 is mainly seen in vascular endothelial cells within infarcted tissues; MMP-1 is detected within cardiomyocytes in the border zone between surviving cardiomyocytes and the infarct. For the morphometric analysis, the expression was assigned a grade of 0 (no expression), 1 (weak expression and focal distribution in <20% of targeted cells), 2 (moderate expression in >20% of targeted cells), or 3 (marked expression and diffuse distribution in >20% of targeted cells) under a high-power field (400×). Grades were assigned to 20–30 high-power fields for each infarcted anterior LV wall. Arrow and arrowheads indicate TGF-β-positive endothelial cells and SDF-1-positive endothelial cells and smooth muscle cells, respectively. Boxed-areas of panel A were highly magnified in panel B.

and produced large infarctions. In the permanent occlusion model, ischemia within the risk areas continues even during the chronic stage; consequently, neovascularization in the form of collaterals is important. On the other hand, in hearts that are reperfused after ischemia, increased neovascularization may be beneficial for the absorption of necrotic tissues and formation of granulation tissue at the subacute stage, but its importance may be reduced at the chronic stage, when the major histological feature is scarring with few cells.

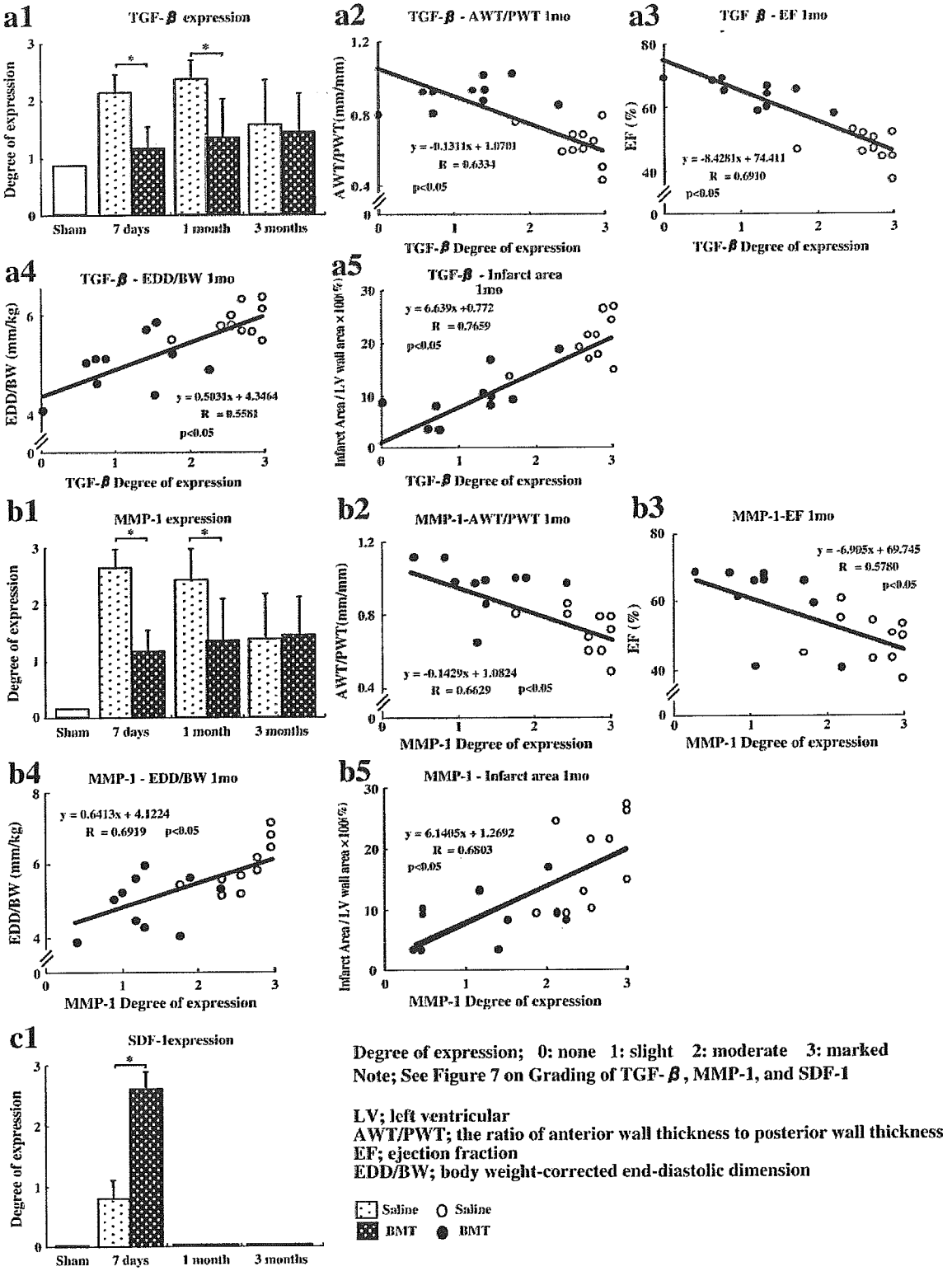

Fig. 8. BM-MNC treatment significantly down-regulated TGF-β and MMP-1 expression 7 days and 1 month post-MI, and up-regulated SDF-1 expression 7 days post-MI (a1, b1 and c1). Levels of TGF-β and MMP-1 were negatively correlated with AWT/PWT ratios and EFs and positively correlated with EDD/BW ratios and infarct size 1 month post-MI (a2–5 and b2–5).

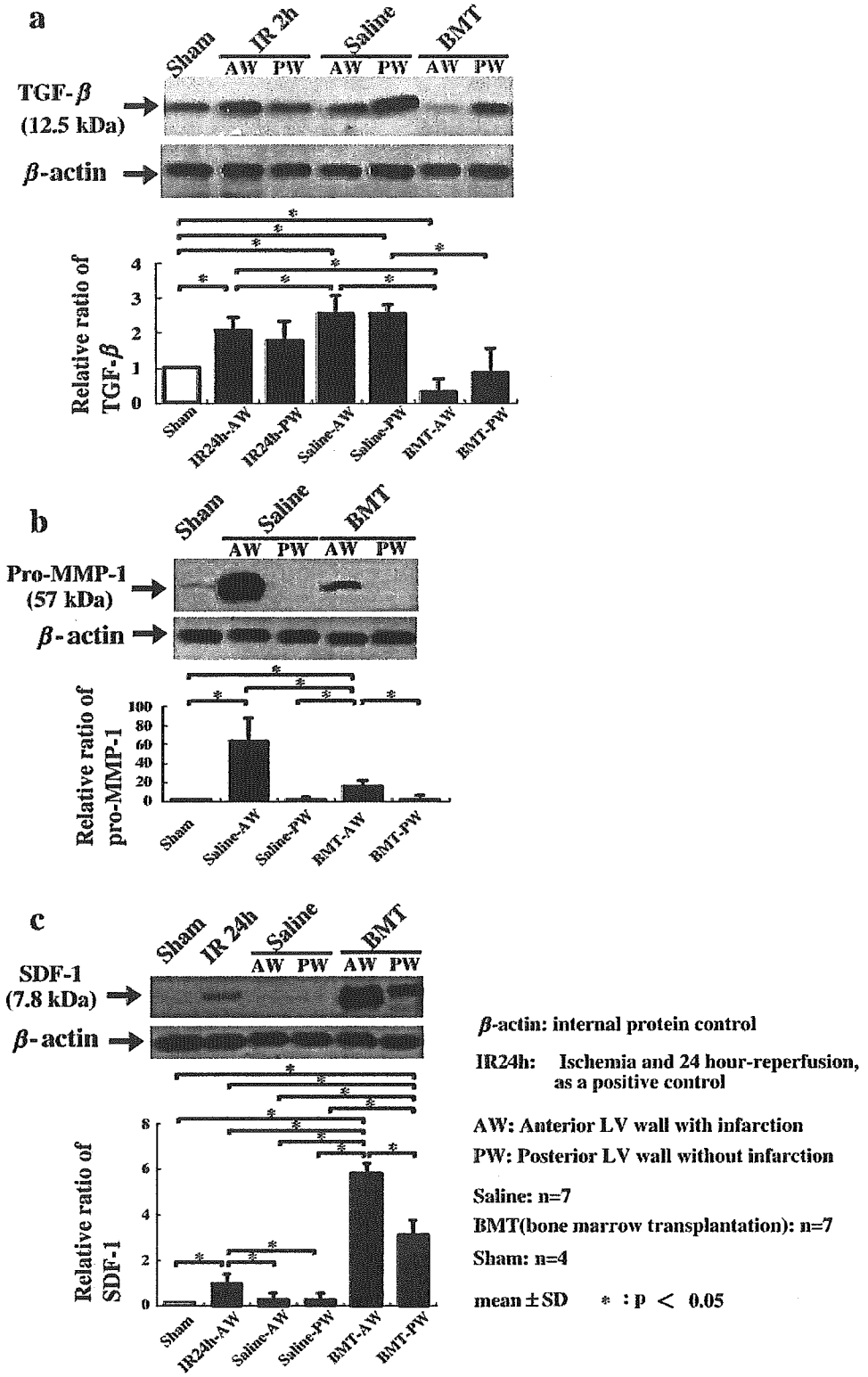

Fig. 9. Western blot analysis 7 days after infarction. Note the up-regulation of TGF-β in both the AW and PW is up-regulated in the Saline group, but down-regulated in the BM-MNC group. Note also that the expression of Pro-MMP-1 in the AW is up-regulated in the Saline, but down-regulated in the BM-MNC group. Finally, note the marked up-regulation of SDF-1 expression in both AW and PW of the BM-MNC group.

4.5. Clinical implications

The clinical implications of the present findings are related to the fact that (1) our model of ischemia–reperfusion corresponds more closely to standard strategies for the treatment of human acute MI than earlier models utilizing permanent occlusion; and that (2) intravenous injection of autologous BM-MNCs is less invasive than direct or intracoronary injection and removes some ethical and technical barriers, such as donor–recipient mismatch and demand–supply imbalance.

In the present study, injected bone marrow cells were aspirated before infarction. However, Dimmeler's group reported that bone marrow mononuclear cells derived from patients with ischemic heart disease showed impaired colony-forming capacity and migratory response to SDF-1 and VEGF. As bone marrow cells after the onset of infarction are available in the clinical setting, our findings based on the bone marrow cells obtained before infarction have limitations.

5. Conclusion

Intravenous transplantation of BM-MNCs leads to the development of BM-MNC-derived myocyte-like cells and regulates the expression of repair-related cytokines that facilitate repair in the post-MI heart.

Acknowledgements

We thank Rumi Maruyama, Akiko Tsujimoto, Hatue Oshika, Kazuko Goto and the staff of Kyoto Women's University (Yumiko Oi, Mayuko Goto, Chitose Suzuki and Yasuyo Hosokawa) for their technical assistance. This study was supported in part by Research Grants of Frontier Medicine (15209027, 16590721) from the Ministry of Education, Science, and Culture of Japan.

Appendix A. Supplementary data

Supplementary data associated with this article can be found, in the online version, at doi:10.1016/j.cardiores.2005.11.001.

References

[1] Orlic D, Kajstura J, Chimenti S, Jakoniuk I, Anderson SM, Li B, et al. Bone marrow cells regenerate infarcted myocardium. Nature 2001; 410:701–5.
[2] Pittenger MF, Martin BJ. Mesenchymal stem cells and their potential as cardiac therapeutics. Circ Res 2004;95:9–20.
[3] Kudo M, Wang Y, Wani MA, Xu M, Ayub A. Implantation of bone marrow stem cells reduces the infarction and fibrosis in ischemic mouse heart. J Mol Cell Cardiol 2003;35:1113–9.
[4] Murry CE, Soonpaa MH, Reinecke H, Nakajima H, Nakajima HO, Rubart M, et al. Haematopoietic stem cells do not transdifferentiate into cardiac myocytes in myocardial infarcts. Nature 2004;428:664–8.
[5] Balsam LB, Wagers AJ, Christensen JL, Kofidis T, Weissman IL, Robbins RC. Haematopoietic stem cells adopt mature haematopoietic fates in ischaemic myocardium. Nature 2004;428:668–73.
[6] Nygren JM, Jovinge S, Breitbach M, Sawen P, Roll W, Hescheler J, et al. Bone marrow-derived hematopoietic cells generate cardiomyocytes at a low frequency through cell fusion, but not transdifferentiation. Nat Med 2004;10:494–501.
[7] Minatoguchi S, Takemura G, Chen X, Wang N, Uno Y, Koda M, et al. Acceleration of the healing process and myocardial regeneration may be important as a mechanism of improvement of cardiac function and remodeling by postinfarction granulocyte colony-stimulating factor treatment. Circulation 2004;109:2572–80.
[8] Ragnarson B, Bengtsson L, Haegerstrand A. Labeling with fluorescent carbocyanine dyes of cultured endothelial and smooth muscle cells by growth in dye-containing medium. Histochemistry 1992;97:329–33.
[9] Honig MG, Hume RI. Fluorescent carbocyanine dyes allow living neurons of identified origin to be studied in long-term cultures. J Cell Biol 1986;103:171–87.
[10] Maruyama R, Takemura G, Aoyama T, Hayakawa K, Koda M, Kawase Y, et al. Dynamic process of apoptosis in adult rat cardiomyocytes analyzed using 48-hour videomicroscopy and electron microscopy-Beating and rate are associated with the apoptotic process. Am J Pathol 2001;159:683–91.
[11] Chacko KJ. Observation on the ultrastructure of developing myocardium of rat embryos. J Morphol 1976;150:681–710.
[12] Alvarez-Dolado M, Pardal R, Garcia-Verdugo JM, Fike JR, Lee HO, Pfeffer K, et al. Fusion of bone marrow-derived cells with Purkinje neurons, cardiomyocytes and hepatocytes. Nature 2003;425:9968–73.
[13] Pochampally RR, Neville BT, Schwarz EJ, Li MM, Prockop DJ. Rat adult stem cells (marrow stromal cells) engraft and differentiate in chick embryos without evidence of cell fusion. Proc Natl Acad Sci U S A 2004;101:9282–5.
[14] Kajstura J, Rota M, Wang B, Cascapera S, Hosoda T, Bearzi C, et al. Bone marrow cells differentiate in cardiac cell lineages after infarction independently of cell fusion. Circ Res 2005;96:127–37.
[15] Barbash IM, Chouraqui P, Baron J, Feinberg MS, Etzion S, Tessone A, et al. Systemic delivery of bone marrow-derived mesenchymal stem cells to the infarcted myocardium: feasibility, cell migration, and body distribution. Circulation 2003;108:863–8.
[16] Yamaguchi J, Kusano KF, Masuo O, Kawamoto A, Silver M, Murasawa S, et al. Stromal cell-derived factor-1 on ex vivo expanded endothelial progenitor cell recruitment for ischemia neovasculalization. Circulation 2003;107:1322–8.
[17] Abbott JD, Huang Y, Liu Dingang, Hickey R, Krause DS, Giordano FJ. Stromal cell-derived factor-1α plays a critical role in stem cell recruitment to the heart after myocardial infarction but is not sufficient to induce homing in the absence of injury. Circulation 2004;110: 3300–5.
[18] Wojakowski W, Tendera M, Michalowska A, Majka M, Kucia M, Maslankiewicz K, et al. Mobilization of CD34/CXCR4$^+$, CD34/CD117$^+$, c-Met$^+$ stem cells, and mononuclear cells expressing early cardiac, muscle, and endothelial markers into peripheral blood in patients with acute myocardial infarction. Circulation 2004;110: 3213–20.
[19] Yelbuz TM, Waldo KL, Zhang X, Waldo K, Zhang X, Zdanowicz M, et al. Myocardial volume and organization are changed by failure of addition of secondary heart field myocardium to the cardiac outflow tract. Dev Dyn 2003;228:152–60.
[20] Deten A, Hoelzl A, Leicht M, Barth W, Zimmer H. Changes in extracellular matrix and in transforming growth factor beta isoforms after coronary artery ligation. J Mol Cell Cardiol 2001;33:1191–207.
[21] Kuwahara F, Kai H, Tokuda K, Kai M, Takeshita A, Egashira K, et al. Transforming growth factor-β function blocking prevents myocardial

fibrosis and diastolic dysfunction in pressure-overloaded rats. Circulation 2002;106:130–5.
[22] Danielsen CC, Wiggers H, Andersen HR. Increased amounts of collagenase and gelatinase in porcine myocardium following ischemia and reperfusion. J Mol Cell Cardiol 1998;30:1431–42.
[23] Spinale FG. Matrix metalloproteinase: regulation and dysregulation in the failing heart. Circ Res 2002;90:520–30.
[24] Kim HE, Dalal SS, Young E, Legato MJ, Weisfeldt ML, D'Armiento J. Disruption of the myocardial extracellular matrix leads to cardiac dysfunction. J Clin Invest 2000;106:857–66.
[25] Gnecchi M, He H, Liang OD, Melo LG, Morello F, Mu H, et al. Paracrine action accounts for marked protection of ischemic heart by Akt-modified mesenchymal stem cells. Nat Med 2005;11:376–468.
[26] Kawamoto A, Gwon H, Iwaguro H, Iwaguro H, Yamaguchi J, Uchida S, et al. Therapeutic potential of ex vivo expanded endothelial progenitor cells for myocardial ischemia. Circulation 2001; 103:634–7.

Original Paper

nephron
Physiology

Nephron Physiol 2006;102:p92–p102
DOI: 10.1159/000090071

Received: November 26, 2004
Accepted: August 17, 2005
Published online: December 6, 2005

Hepatocyte Growth Factor Gene Therapy Slows Down the Progression of Diabetic Nephropathy in *db/db* Mice

Tomoyo Kagawa[a] Genzou Takemura[a] Ken-ichiro Kosai[b] Ichijiro Murata[a, c]
Takamasa Ohno[c] Tomoyuki Takahashi[b] Masayasu Esaki[a, b] Rumi Maruyama[a]
Takako Fujiwara[d] Hiroshige Ohashi[e] Hisayoshi Fujiwara[a]

Departments of [a]Internal Medicine, [b]Gene Therapy and Regenerative Medicine, and [c]Oriental Medicine, Gifu University School of Medicine, Gifu; [d]Department of Food Science, Kyoto Women's University, Kyoto, and [e]Division of Nephrology, Gifu Prefectural Gifu Hospital, Gifu, Japan

Key Words
Diabetes · Apoptosis · Nephropathy · Growth factors · Gene therapy

Abstract
Background: Effect of hepatocyte growth factor (HGF) has scarcely been determined on diabetic nephropathy. ***Methods:*** Adenovirus encoding human HGF gene or LacZ gene (as the control) was injected into the hindlimb muscles of the C57BL/KsJ-*db/db (db/db)* mice at the age of 12 weeks, a model of genetic diabetes. Diabetic nephropathy was then evaluated at the age of 24 weeks. ***Results:*** The urine volume and albumin excretion progressively decreased in the control, whereas they remained unchanged in the HGF-treated group during the 12-week follow-up. The HGF gene therapy did not affect glucose metabolism. However, it resulted in a better renal function as evaluated by creatinine clearance (Ccr) than the control; Ccr was progressively worsened in controls (0.14 ± 0.02 liters/day) whereas unchanged in the HGF gene-treated group (0.38 ± 0.09 liters/day, $p < 0.05$). Kidneys of the HGF gene-treated mice showed glomeruli with greater area and cell population, smaller glomerular sclerotic index, and less fibrosis in both glomeruli and renal tubules, where apoptotic rate of glomerular endothelial cells and that of tubular epithelial cells were significantly decreased. TGF-β1 expression was significantly decreased in kidneys of the HGF gene-treated group. Finally, the HGF treatment significantly improved the long-term survival of *db/db* mice. ***Conclusions:*** The HGF gene delivery thus appeared to slow down the aggravation of diabetic nephropathy in *db/db* mice by attenuating progression from the hyperfiltration phase into the sclerotic phase through antiapoptotic and antifibrotic actions. The present findings suggest that the HGF gene delivery can be a novel therapeutic approach against diabetic nephropathy.

Introduction

Diabetic nephropathy is one of the most problematic renal diseases because of the exponentially increasing number of patients entering chronic dialysis programs with renal failure resulting from diabetes, and the high mortality rates of these patients receiving dialysis [1]. Diabetic nephropathy, in addition to many other glomerular diseases, finally progresses into a hypocellular, sclerotic phase. One of the most conspicuous pathologic changes in glomeruli of this disorder is mesangial expansion ac-

KARGER
Fax +41 61 306 12 34
E-Mail karger@karger.ch
www.karger.com

1660–2137/06/1024–0092$23.50/0

Accessible online at:
www.karger.com/nep

Hisayoshi Fujiwara, MD, PhD
Second Department of Internal Medicine
Gifu University School of Medicine
1-1 Yanagido, Gifu 501-1194 (Japan)
Tel. +81 58 230 6520, Fax +81 58 230 6521, E-Mail gifuim-gif@umin.ac.jp

companied by mesangial matrix deposition that consists of collagen and glycoproteins [2, 3]; such excessive deposits are, at least in part, associated with overexpression of transforming growth factor-β (TGF-β) [4, 5]. In addition, apoptosis was documented in tubular epithelial cells, which may contribute to atrophy of tubular epithelium and tubulointerstitial fibrosis in diabetic nephropathy [6, 7]. Moreover, we recently reported an increased apoptosis of renal glomerular cells of the Otsuka Long-Evans Tokushima Fatty (OLETF) rat, an animal model of non-insulin-dependent diabetes mellitus [8]. Thus, both space occupation by mesangial matrix and cell loss via apoptosis could importantly account for glomerular sclerosis with decreased capillaries in diabetic nephropathy.

Hepatocyte growth factor (HGF), originally identified and cloned as a potent mitogen for hepatocytes [9, 10], shows potent angiogenic and mitogenic activities in various cells, preferentially in most epithelial and endothelial cells [11, 12]. In addition to this, antiapoptotic and antifibrotic activities of HGF have recently been paid attention; its antiapoptotic effect was accompanied by activation of the phosphatidylinositol 3-kinase/Akt pathway [13, 14], while its antifibrotic effect was reported to work through the antagonistic action on TGF-β [15]. The therapeutic efficacy of HGF was actually confirmed on renal fibrosis caused by chronic glomerulonephritis or by urinary obstruction [16–18]. Recently, Mizuno et al. [19] found beneficial effects of a long-term treatment with recombinant HGF upon streptozotocin-induced diabetic nephropathy in mice. Moreover, Cruzado et al. [20] demonstrated that HGF gene therapy not only prevents but also reverts advanced diabetic nephropathy in the same animal model. Except for these studies, however, effects of HGF on diabetic nephropathy have scarcely been determined and not confirmed in the other animal models. In the present study, we examined the effects of HGF gene therapy with adenovirus encoding the human HGF gene on progression of diabetic nephropathy, glomerular sclerosis in particular. We used the C57BL/KsJ-*db/db (db/db)* mouse, a rodent model of genetic diabetes, which exhibits renal pathology and dysfunction resembling those observed in human diabetes [21–23].

Materials and Methods

Animals

All procedures were in accordance with institutional guidelines for animal research. Female 8-week-old diabetic C57BL/KsJ-*db/db (db/db)* mice were purchased from Clea Japan (Tokyo, Japan). Mice were designated *db/db* by the vendor on the basis of the appearance of obesity, which is usually detectable at about 5 weeks of age. As the non-diabetic control mice, C57BL/KsJ-*db/+m (db/+m)* mice with the same sex and age were used (Clea Japan). Animals were weighed on receipt and weekly thereafter, and were provided food and water ad libitum.

Recombinant Adenoviral Vectors

Adenoviral vector plasmid pAd-HGF, which comprises cytomegalovirus immediate early enhancer, a modified chicken β-actin promoter and human HGF cDNA (Ad.CAG-HGF) was constructed by the in vitro ligation method (from Dr. Mark A. Kay, Stanford University School of Medicine) as described previously [24]. Control Ad-LacZ was prepared as described previously [25].

Ad.CAG-HGF (1×10^9 plaque-forming units [pfu]/mouse) was injected into the hindlimb muscles of the 12-week-old *db/db* mice (n = 8) and *db/+m* mice (n = 6). As the control, an adenovirus encoding the LacZ gene (Ad.CAG-LacZ) was similarly injected to the other 8 *db/db* and 6 *db/+m* mice. Mice were followed-up for 12 weeks. They were killed by cervical dislocation and examined at the age of 24 weeks.

Urine and Blood Examination

Twenty-four-hour urine collections were periodically obtained in each animal after placement in a metabolic cage by washing the collection apparatus with 10 ml of distilled water with a spray bottle. Approximately 50–100 μl blood was obtained from the tail veins.

Glucose, albumin, creatinine, blood urea nitrogen (BUN), and HbA1c in blood and/or urine were measured by the standardized methods.

Measurement of Human HGF Level in the Plasma

The plasma concentration of human HGF was measured using an ELISA kit (Bethyl Laboratories, Montgomery, Tex., USA).

Histological Examination

The kidney was fixed in 10% phosphate-buffered formalin solution, and embedded in paraffin. Sections of 4 μm thickness were cut and stained with hematoxylin and eosin, PAS, and Sirius red F3BA (0.1% solution in saturated aqueous picric acid) (Aldrich Chemicals, Milwaukee, Wisc., USA) [26]. The glomerular size was measured as the whole capillary tuft area using a computed image analyzer (LUZEX F, Nireco Co., Kyoto, Japan) for 50 glomeruli on each slide under light microscopy. The cell number in each glomerulus (n = 50) was calculated using preparations stained with hematoxylin and eosin. Glomerular sclerotic index was calculated as the percent of the PAS-positive area in the glomerular area in preparations stained with PAS [27].

Immunohistochemistry

On the 4-μm-thick sections, proliferating cell nuclear antigen (PCNA) and Flk-1 were immunohistochemically stained using ABC Elite kits (Vector, Burlingame, Calif., USA). The primary antibodies used were anti-PCNA antibody (clone PC10, Dako Japan, Kyoto, Japan) at a dilution of 1:100 and anti-Flk-1 antibody (clone A-3, Santa Cruz, Calif., USA) at 1:100. Pretreatment by microwave irradiation in 10 m*M* citrate buffer (pH 6.0) at 400 W for 5 min twice was performed to retrieve the antigenicities. Diaminobenzidine tetrahydrochloride (DAB) or VIP substrate (Vector) was the chromogen. Mouse intestine was used as the positive control tissue

sections. Unanimity on the positive immunohistochemical stainings was acquired for all sections between the two observers who were unaware of which group the sections belonged.

In situ Nick End Labeling (TUNEL)

TUNEL was performed in deparaffinized 4-μm-thick sections with an ApopTag kit (Intergene, Purchase, N.Y., USA) according to the supplier's instructions. DAB was the chromogen. Sections were then counterstained with hematoxylin.

Double Immunohistochemistry

Sections were stained first with anti-PCNA antibody or TUNEL as described above. Then the sections were stained with the second primary antibody against Flk-1 and visualized with VIP substrate.

Electron Microscopy

Tissue samples of the kidney were cut into 1-mm cubes and fixed for 4 h at 4°C in 2.5% glutaraldehyde in 0.1 mol/l phosphate buffer. They were postfixed in 1% buffered osmium tetroxide, dehydrated through graded ethanols, and embedded in Epon. Thin sections (80 nm) were cut with a diamond knife, collected on 300-mesh copper or nickel grids, and double stained with uranyl acetate and lead citrate before examination using an electron microscope (H-700, Hitachi, Tokyo, Japan). Ten photographs were taken in each glomerulus with a magnification of ×3,000 and printed. Five points of glomerular basement membrane picked up in each photograph and the thickness was measured. 100–150 measurements were averaged on 2–3 glomeruli per specimen.

Western Blotting for TGF-β1

Fifty micrograms of protein from fresh kidney homogenates in sample buffer (0.4 mol/l Tris-HCl, pH 6.8, 10% glycerol, 2% SDS, 0.02% bromophenol blue, and 2.5% 2-mercaptoethanol) was loaded per lane on 12 or 16% polyacrylamide gels and electrophoresed. Proteins were transferred, and the membranes were incubated with primary antibody using a 1:1,000 dilution of anti-TGF-β1 antibody (Promega, Madison, Wisc., USA). Alpha-tubulin was the loading control. The membranes were incubated with a 1:2,000 dilution of horseradish peroxidase-conjugated goat anti-mouse or anti-rabbit immunoglobulin (Amersham, UK). Immunoblots were developed by enhanced chemiluminescence system (ECL; Amersham Biosciences, Piscataway, N.J., USA) and exposed to imaging film (X-X-OMAT; Kodak, Rochester, N.Y., USA). The signals were quantified by densitometry.

Survival Study

For the survival study, female 12-week-old *db/db* mice were injected intramuscularly with Ad.CAG-HGF (1×10^9 pfu/mouse) (n = 15) or LacZ gene (1×10^9 pfu/mouse) (n = 15) and followed for 25 weeks.

Statistical Analysis

Values were expressed as the means ± SEM. Statistical comparisons were performed by Student's t test. Survival data were analyzed by the Kaplan-Meier method. $p < 0.05$ was considered significant.

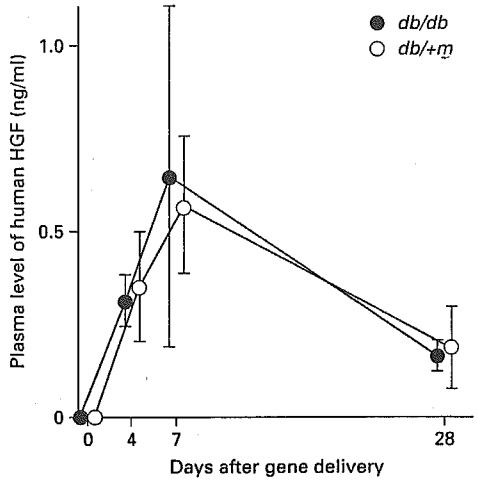

Fig. 1. Time course of human HGF levels in plasma of *db/db* and *db/+m* mice after HGF gene delivery. n = 3–6 at each time point in each group. In plasma of mice treated with LacZ gene, no HGF was detectable.

Results

Plasma Levels of Human HGF

As shown in figure 1, plasma human HGF was detectable after the HGF gene delivery in *db/db* and *db/+m* mice, whereas no human HGF was detected in the LacZ-treated mice. The plasma levels of human HGF in the *db/+m* mice after the HGF gene delivery were similar to those in the *db/db* mice (fig. 1). Effective bioactivity of human HGF on mice was confirmed in a previous study [28].

Renal Function

The blood glucose and HbA1c levels in *db/+m* and *db/db* mice were not significantly different between the LacZ- and HGF-treated groups at the age of 24 weeks (table 1), indicating no significant effect of the HGF gene delivery on glucose metabolism in these mice.

Figure 2 shows data of urine and blood chemistry on renal function in the LacZ- and HGF-treated *db/+m* and *db/db* mice before (at the age of 12 weeks) and at 12 weeks after the treatment (at the age of 24 weeks). As shown here, the *db/db* mice display far greater urine volume,

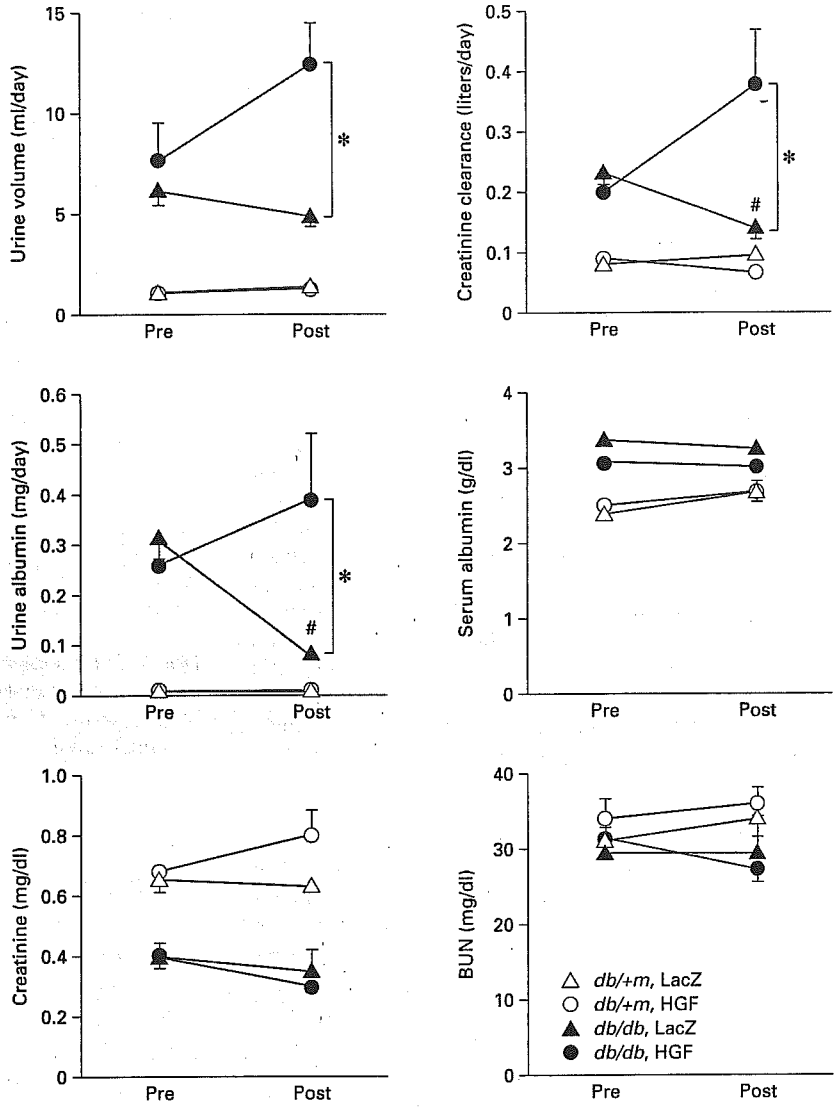

Fig. 2. Parameters of renal function in *db/db* and *db/+m* mice before and after LacZ- or HGF-gene therapy. # $p < 0.05$ compared with the pretreatment value. * $p < 0.05$ compared with the corresponding value of the LacZ group.

Table 1. Blood glucose and HbA1c values at the post-treatment with LacZ or HGF gene in *db/+m* and *db/db* mice

	db/+m		*db/db*	
	LacZ	HGF	LacZ	HGF
n	6	6	8	8
Blood glucose, mg/dl	201±11	211±8	836±33	801±26
HbA1c, %	2.8±0.11	2.9±0.06	13.7±0.2	12.9±0.3

greater urine albumin amount and concentration, smaller concentrations of serum creatinine and BUN, and greater creatinine clearance (Ccr), compared with the *db/+m* mice.

Although the HGF gene delivery did not affect any functional parameters of the *db/+m* mice, the renal function was significantly affected by the treatment in the *db/db* mice. Urine volume per day was greater in the HGF-treated *db/db* mice than in the LacZ-treated ones. Although urine albumin concentration was similar between the groups at the post-treatment, urine albumin amount was greater in the HGF-treated group; this is

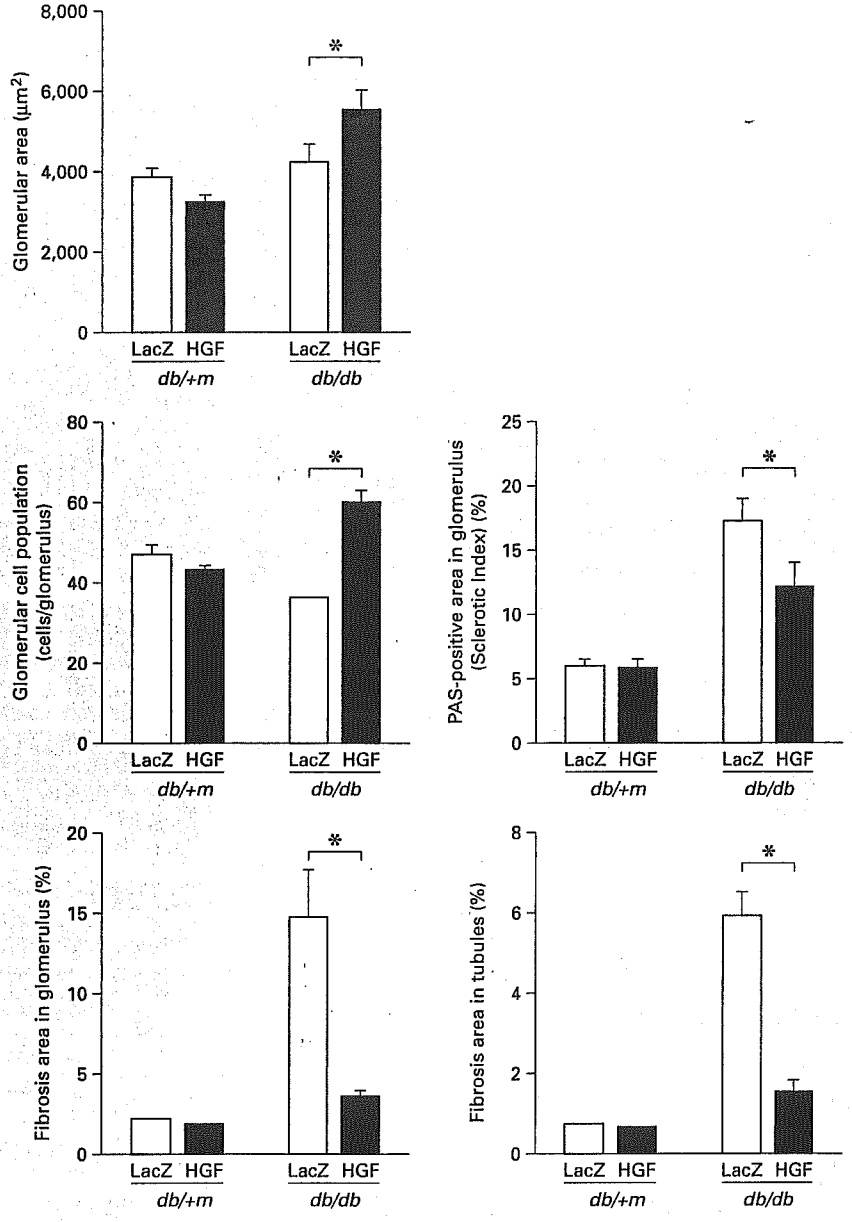

Fig. 3. Parameters of renal pathology in *db/db* and *db/+m* mice after LacZ or HGF gene treatment. * $p < 0.05$.

probably attributed in part to the greater amount of urine volume in that group. Serum albumin concentration was similar between the groups. Neither serum creatinine nor BUN level was significantly different between the groups at the age of 24 weeks, but the Ccr was significantly greater in the HGF-treated group; this value was worsened in the LacZ-treated group at the age of 24 weeks than at the age of 12 weeks, whereas in the HGF-treated group the value showed no significant change during the interval. These findings suggested that the glomerular hyperfiltration phase progressed into the sclerotic phase of nephropathy during the treated period for 12 weeks, in the control (LacZ-treated) *db/db* mice, while the progression was decelerated in the HGF-treated *db/db* mice.

Renal Pathology

Figure 3 shows quantitative data on renal pathology of the 24-week-old *db/+m* and *db/db* mice at the post-treatment with LacZ or HGF gene. The data were not different between treatments in the *db/+m* mice, where-

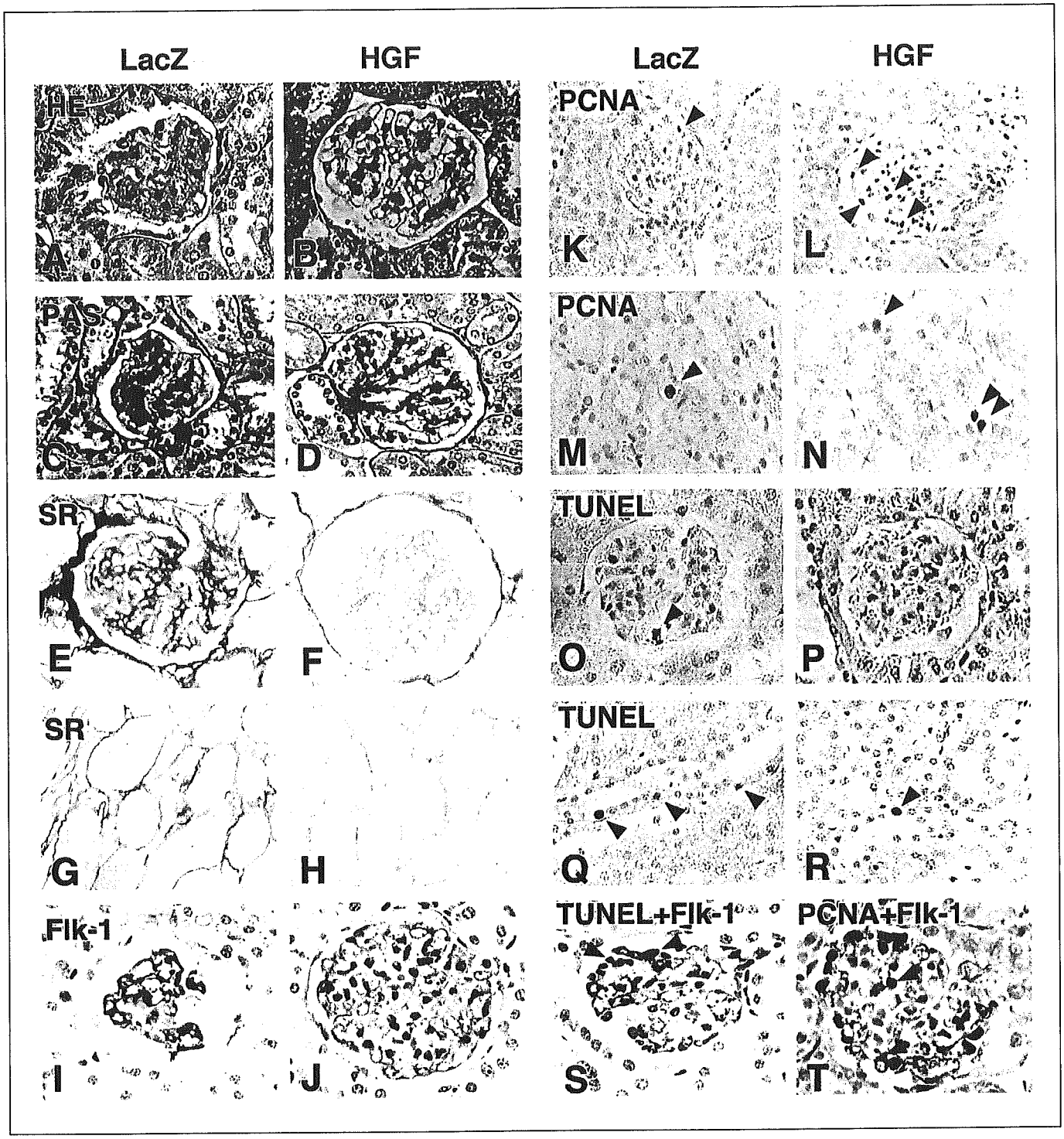

Fig. 4. Light microphotographs of renal glomeruli or tubules of *db/db* mice treated with LacZ (**A**, **C**, **E**, **G**, **I**, **K**, **M**, **O**, **Q**, **S**) or with HGF (**B**, **D**, **F**, **H**, **J**, **L**, **N**, **P**, **R**, **T**). **A**, **B** Hematoxylin-eosin stain. **C**, **D** PAS stain. **E–H** Syrius red stain. **I**, **J** Immunostain for Flk-1. **K–N** Immunostain for PCNA. **O–R** TUNEL stain. **S** TUNEL combined with Flk-1 immunostain. **T** Double immunostain for PCNA and Flk-1. Arrows indicate immunopositive cells. Original magnifications: ×400 in **S** and **T**; ×200 in the other panels.